50 dB parametric on-chip gain in silicon photonic wires

Bart Kuyken,[1,†] Xiaoping Liu,[2,4,†] Günther Roelkens,[1] Roel Baets,[1] Richard M. Osgood, Jr.,[2] and William M. J. Green[3,*]

[1]*Photonics Research Group, Department of Information Technology, Ghent University—imec, Ghent B-9000, Belgium*

[2]*Department of Electrical Engineering, Columbia University, 1300 S. W. Mudd Building, 500 W. 120th Street, New York, New York 10027, USA*

[3]*IBM Thomas J. Watson Research Center, 1101 Kitchawan Road, Yorktown Heights, New York 10598, USA*

[4]*Current address: OFS Labs, 19 Schoolhouse Road, Somerset, New Jersey 08873, USA*

**Corresponding author: wgreen@us.ibm.com*

Received June 9, 2011; revised October 3, 2011; accepted October 4, 2011;
posted October 7, 2011 (Doc. ID 148981); published November 15, 2011

A pulsed mid-infrared pump at $\lambda = 2173$ nm is used to demonstrate wideband optical parametric gain in a low-loss 2 cm long silicon photonic wire. Using dispersion engineering to obtain negative second-order (β_2) and positive fourth-order (β_4) dispersion, we generate broadband modulation instability and parametric fluorescence extending from 1911 nm–2486 nm. Using a cw probe signal to interrogate the modulation instability spectrum, we demonstrate parametric amplification >40 dB with an on-chip gain bandwidth wider than 580 nm, as well as narrowband Raman-assisted peak gain >50 dB. © 2011 Optical Society of America

OCIS codes: 130.4310, 190.4380, 190.4970.

Two-photon absorption (TPA) in Si vanishes at wavelengths approaching $\lambda = 2200$ nm, while its nonlinear Kerr refractive index n_2 stays comparatively constant [1]. Hence, the nonlinear figure of merit ($n_2/\beta\lambda$) increases dramatically near silicon's TPA threshold. The large intrinsic nonlinearity of Si, when patterned into high-index-contrast dispersion-engineered silicon photonic wires, produces an ideal platform for the exploration of highly efficient, broadband, coherent nonlinear optical processes [2,3]. This platform can serve as an ideal host for chip-scale mid-IR applications [4–7], including molecular spectroscopy, free-space communication, and environmental monitoring.

Previously we reported a mid-IR optical parametric amplifier (OPA) with on-chip gain over a 220 nm bandwidth in a 4 mm long silicon wire [4]. Using an improved design, here we demonstrate broadband mid-IR modulation instability (MI), having a bandwidth greater than 580 nm centered at a 2173 nm pump wavelength. The intense MI spectrum correlates with unprecedented values of on-chip parametric gain, exceeding 40 dB. Moreover, we demonstrate that on-chip gain exceeds 50 dB in narrow Raman-scattering-assisted bands.

To achieve an efficient degenerate four-wave-mixing (FWM) process (i.e., $2\omega_p = \omega_s + \omega_i$, where ω_p, ω_s, and ω_i are the pump, signal, and idler angular optical frequencies), the phase-matching condition [8] restricts the frequency detuning of signal/idler from pump $\Delta\omega = |\omega_p - \omega_s| = |\omega_p - \omega_i|$ to values that satisfy $|\Delta k_l + 2\gamma P| \le (4\gamma PL)^{1/2}/L$ or $2\gamma P - (4\gamma PL)^{1/2}/L \le -\Delta k_l \le 2\gamma P + (4\gamma PL)^{1/2}/L$. Here, Δk_l is the linear phase-mismatch in propagation constants between signal/idler and pump, $\Delta k_l = (k_s + k_i) - 2k_p$, γ is the waveguide's effective nonlinearity parameter, P is the input pump peak power and L is the waveguide length. Graphically, when the $-\Delta k_l$ curve falls into a band bounded between $2\gamma P - (4\gamma PL)^{1/2}/L$ and $2\gamma P + (4\gamma PL)^{1/2}/L$ (i.e., the horizontal hatched bands in Fig. 1), efficient phase matching is achieved. Using a Taylor series, $-\Delta k_l$ can be related to $\Delta\omega$ through $-\Delta k_l \approx -\beta_2(\Delta\omega)^2 - \beta_4(\Delta\omega)^4/12$, where β_2 and β_4 are the waveguide's second-order and fourth-order dispersion coefficients, respectively. Figure 1 schematically illustrates a typical phase-matching relationship for $\beta_2 < 0$ and $\beta_4 > 0$. The solid black curve depicting $-\Delta k_l$ initially increases, reaches a peak, and then decreases with increasing frequency detuning from the pump. At low power levels, there exist two phase-matched regions (i.e., intersecting with the horizontal black hatched band in Fig. 1), as shown by the solid black and the dashed black arrow. At small frequency detuning, a "broadband" gain region typically seen in parametric amplification [2–4] is found. At large frequency detuning, the gain has a narrower bandwidth, termed here a "discrete" band [9–11] due to the relatively large slope of $-\Delta k_l$. When the pump power is increased (i.e., from black to the red hatched bands), the broadband and discrete phase-matched bands shift closer together. At high pump power levels these two regions eventually merge together to create a single ultrabroadband phase-matched region, depicted by the dotted blue arrow and blue hatched band.

We performed a series of FWM experiments to investigate the bandwidth and magnitude of parametric gain and wavelength conversion when operating within the ultrabroadband phase-matching region. Our Si wire is fabricated on a 200 mm silicon-on-insulator wafer in a complementary metal–oxide–semiconductor pilot line and is 2 cm long, with cross-sectional dimensions of 900 nm × 220 nm. The top/bottom cladding consist of air/2 μm buried oxide, respectively. The waveguide operates in the fundamental quasi-TE mode, with propagation

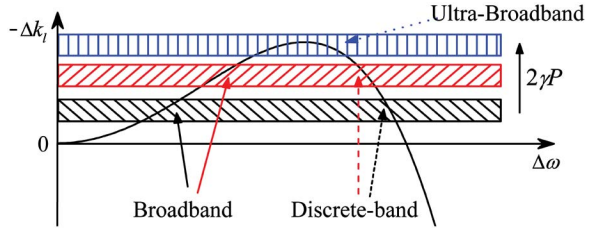

Fig. 1. (Color online) Schematic illustration of pump-detuning-dependent broadband, discrete-band, and ultrabroadband phase-matched regions for FWM. The horizontal black, red, and blue hatched bands correspond to conditions with increasing pump power.

losses of <2.8 dB/cm for $\lambda = 2000$–2500 nm, and has a γ parameter $\sim 150\,(\mathrm{W \cdot m})^{-1}$. The Si wire is pumped with a picosecond pulse train at $\lambda = 2173$ nm (FWHM~2 ps, repetition rate = 76 MHz) from an OPA. The polarization of the pump and probe are controlled to coexcite the Si wire's quasi-TE mode using in-line fiber polarization controllers. The pump and probe are multiplexed with a 90/10 fused-fiber coupler. Coupling into/out of the Si wire is via lensed fibers, with coupling losses of ~10 dB/facet. An optical spectrum analyzer is used to record the input/output spectra at 1 nm resolution bandwidth.

The dashed magenta trace in Fig. 2(a) depicts the pump spectrum at the input of the Si wire. The pump has an instrumentation-limited signal-to-noise ratio >75 dB, and a peak on-chip power of $P \sim 13.5$ W. The pump's transmission spectrum obtained at the wire output [solid blue curve in Fig. 2(a)] exhibits features commonly observed for pulse propagation through Si waveguides, these being self-phase modulation-induced (SPM) spectral oscillations on the original pump spectrum, and a blueshift due to residual free-carrier dispersion [12,13]. The transmitted pump spectrum also exhibits additional modifications, several of which are observed here for the first time in Si wires. Most notably, the output spectrum is characterized by the emergence of a strong ultrabroadband MI background [8,14], extending from 1911 to 2486 nm. Furthermore, a prominent Raman Stokes peak, downshifted from the pump by ~15.6 THz [7], rides on top of the MI spectrum at $\lambda = 2411$ nm. Finally, a coherent Raman anti-Stokes [15] peak is visible at a wavelength of 1950 nm. Strong Raman interaction occurs within the Si waveguide after SPM-induced spectral narrowing significantly compresses the –3 dB bandwidth of the negatively chirped input pulse from ~740 GHz to ~140 GHz [9], a value comparable to the spectral bandwidth of Raman scattering in Si. Sharp interference fringes occur near the Raman peaks, where the dispersion and phase shift due to the Raman susceptibility disrupts the broadband FWM phase-matching condition [16].

Figure 2(b) shows a series of pump-power-dependent MI spectra. With increasing pump power, the centers of the broadband MI peaks move away from the pump (dashed red arrows), while the narrower discrete MI peaks move closer to the pump (solid black arrows), an observation consistent with the schematic in Fig. 1. Using the observed detuning $\Delta\omega$ of MI peaks from pump, along with the values of the pump-power-dependent nonlinear phase shift $2\gamma P$, we generate an experimental fit describing the Si wire's dispersion coefficients (as outlined in [17]). At the pump wavelength of 2173 nm, β_2 and β_4 are estimated to be $-0.6\,\mathrm{ps}^2/\mathrm{m}$ and $5.1 \times 10^{-4}\,\mathrm{ps}^4/\mathrm{m}$, respectively. While the β_2 value is reasonably close to the value of $-0.52\,\mathrm{ps}^2/\mathrm{m}$ obtained from simulations, the β_4 is an order of magnitude larger than numerically predicted. This deviation is primarily due to the fact that the simulations do not capture the nanometer-scale fabrication tolerances in the wire's cross-sectional dimensions [17], which have a significant impact on higher-order dispersion.

The visibility of a strong noise-seeded spontaneous emission/MI background suggests that the on-chip mid-IR parametric gain available here is far larger than that demonstrated in previous studies [4], where no such MI was observed. As shown by the overlaid spectra in Fig. 3(a), the parametric amplification is probed using a cw signal with wavelengths varying from 2209 nm–2498 nm (8 nm step size), thus generating the corresponding idler terms from 2129 nm–1914 nm. The cw signal power coupled into the waveguide is kept low (<0.06 mW) to prevent pump depletion, yet high enough to achieve visibility of the idler above the MI spectrum. The pedestal around the cw signals in Fig. 3(a) is formed by the amplified pulsed signal, and its height relative to the cw signal on the spectra is roughly proportional to the on-chip gain [4]. Figure 3(b) plots the measured on-chip amplification and conversion gain, defined as the ratio between the peak power of pulsed signal/idler at the end of the waveguide and the coupled input cw signal power (see [4] for details). The mid-IR-pumped Si wire OPA exhibits on-chip optical parametric amplification over a bandwidth exceeding 580 nm. Within the Raman Stokes/anti-Stokes bands, the OPA reaches a maximum value of Raman-assisted parametric signal/idler gain of ~50 dB. Note that

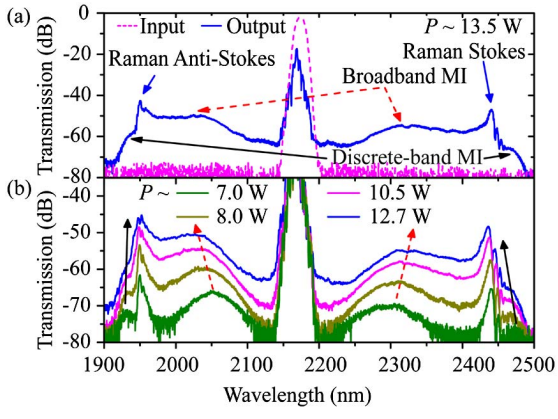

Fig. 2. (Color online) (a) Input (dashed magenta) and output (solid blue) pump spectrum, taken with an input peak power $P \sim 13.5$ W and $\lambda = 2173$ nm, illustrating ultrabroadband MI, and Raman Stokes/anti-Stokes peaks. (b) MI spectra with four different pump peak power levels at pump wavelength $\lambda = 2173$ nm.

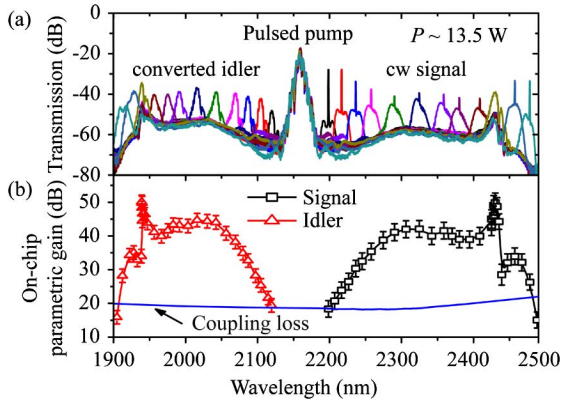

Fig. 3. (Color online) (a) Series of FWM spectra with the pulsed pump copropagating with a cw mid-IR signal at various wavelengths. The pulsed pump is centered at $\lambda = 2173$ nm, and has $P \sim 13.5$ W. (b) Spectrum of on-chip parametric signal gain (black squares) and idler conversion gain (red triangles). Fiber-waveguide coupling loss measured with cutback method is shown by the blue trace.

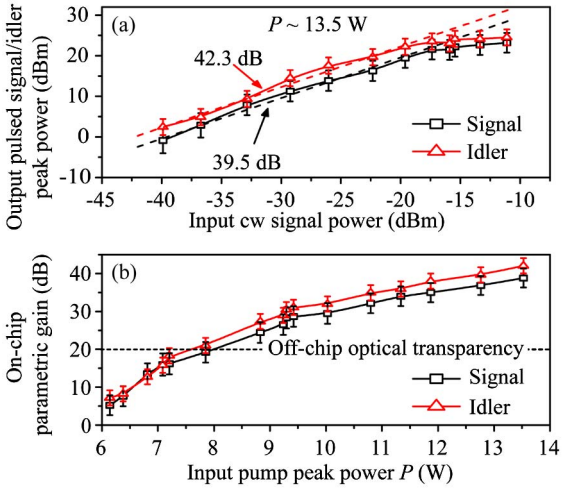

Fig. 4. (Color online) (a) Output pulsed signal/idler peak power versus input cw signal power at $\lambda_s = 2356$ nm, with input pump peak power $P \sim 13.5$ W. (b) On-chip parametric gain as a function of P. Off-chip optical transparency is achieved with a peak power of ~8 W.

the gain profile also contains interference patterns near the Raman-assisted peaks, at wavelengths of ~2445 nm and ~1950 nm. These features are related to those seen in the MI spectrum of Fig. 2(a). However, the number of interference fringes observed in Fig. 3(b) is reduced, because the cw probe's linewidth is broadened by cross-phase modulation [12], in combination with the limited resolution of the 8 nm probe tuning step. After compensating for all fiber-chip coupling losses (~20 dB), the OPA shows a net off-chip gain bandwidth of ~550 nm, with ~30 dB Raman-assisted peak off-chip gain for both signal and idler. The off-chip parametric amplification resulting solely from FWM can be >20 dB.

Large values of on-chip parametric amplification can lead to pump depletion [8] and even gain saturation at high input signal power. This is seen in a plot of output pulsed signal/idler peak power versus input cw signal power shown in Fig. 4(a). Here the input pump peak power is $P \sim 13.5$ W. The signal wavelength is positioned near the FWM parametric gain maximum ($\lambda_s = 2356$ nm), but outside the Raman band. At low signal-power levels, the power of the amplified signal and converted idler increase linearly with signal power, resulting in a signal and idler on-chip parametric gain of 39.5 and 42.3 dB, respectively. The output signal/idler power saturates at ~20 dBm, for input signal powers > – 19 dBm. This gain saturation can be useful for limiting all-optical regeneration of signals [3].

Figure 4(b) plots the signal/idler on-chip parametric gain versus input peak pump power while keeping the signal wavelength at $\lambda_s = 2356$ nm and its power at –23.3 dBm. After compensating for the 20 dB coupling loss, off-chip optical transparency can be achieved for a peak pump power about 8 W, which can be further reduced by improving upon the cleaved-facet input coupling mechanism used here. The differential gain is about 10.4 dB/W at low peak power ~6.5 W but decreases to 2.7 dB/W for a peak power >10 W. This decrease is in part due to the residual nonlinear loss [4,18]. However, as shown in Fig. 4(b), even at the highest peak power, the on-chip parametric gain does not fully saturate, but rather continues to grow with a reduced differential gain.

The results obtained here represent a substantial improvement over those reported previously for mid-IR parametric amplification in a 4 mm long silicon wire waveguide [4]. The peak operating pump power is reduced to less than half in the present device. At the same time, the maximum on-chip gain obtained using this 2 cm long wire here shows an improvement of more than 25 dB, while the on-chip gain bandwidth is increased by more than 2.5×. These results were achieved by leveraging judicious dispersion engineering and reduced propagation loss in the silicon wires, to achieve dramatic increase in parametric gain and its bandwidth, including phase matching of the Raman scattering process.

X. Liu and R. Osgood would like to thank Sebastian Doetsch for many useful discussions during his stay in the U.S. X. Liu thanks IBM for financial support, R. Osgood thanks the National Science Foundation (NSF) (Award ID 0806682) for supporting this project. B. Kuyken acknowledges the Research Foundation—Flanders (FWO) for a research grant. This work was also supported by the FP7-ERC projects MIRACLE and InSpectra. The authors also thank Yurii A. Vlasov at IBM Research for his support.

†These authors contributed equally to this work.

References

1. A. D. Bristow, N. Rotenberg, and H. M. van Driel, Appl. Phys. Lett. **90**, 191104 (2007).
2. M. A. Foster, A. C. Turner, J. E. Sharping, B. S. Schmidt, M. Lipson, and A. L. Gaeta, Nature **441**, 960 (2006).
3. R. Salem, M. A. Foster, A. C. Turner, D. F. Geraghty, M. Lipson, and A. L. Gaeta, Nat. Photon. **2**, 35 (2008).
4. X. P. Liu, R. M. Osgood, Y. A. Vlasov, and W. M. J. Green, Nat. Photon. **4**, 557 (2010).
5. S. Zlatanovic, J. Park, S. Moro, J. Boggio, I. Divliansky, N. Alic, S. Mookherjea, and S. Radic, Nat. Photon. **4**, 561 (2010).
6. R. Lau, M. Menard, Y. Okawachi, M. Forst, A. Turner-Foster, R. Salem, M. Lipson, and A. Gaeta, Opt. Lett. **36**, 1263 (2011).
7. V. Raghunathan, D. Borlaug, R. R. Rice, and B. Jalali, Opt. Express **15**, 14355 (2007).
8. G. P. Agrawal, *Nonlinear Fiber Optics* (Academic, 2001).
9. Q. Lin, T. J. Johnson, R. Perahia, C. P. Michael, and O. J. Painter, Opt. Express **16**, 10596 (2008).
10. E. K. Tien, Y. W. Huang, S. M. Gao, Q. Song, F. Qian, S. K. Kalyoncu, and O. Boyraz, Opt. Express **18**, 21981 (2010).
11. B. Kuyken, X. Liu, R. Osgood, Y. Vlasov, G. Roelkens, R. Baets, and W. Green, *Proceedings of the Optical Fiber Communication Conference (OFC) 2011* (Optical Society of America, 2011), paper OTU4.
12. J. Dadap, N. Panoiu, X. G. Chen, I. W. Hsieh, X. P. Liu, C. Y. Chou, E. Dulkeith, S. McNab, F. Xia, W. Green, L. Sekaric, Y. A. Vlasov, and R. M. Osgood, Opt. Express **16**, 1280 (2008).
13. X. P. Liu, J. Driscoll, J. Dadap, R. M. Osgood, S. Assefa, Y. A. Vlasov, and W. M. J. Green, Opt. Express **19**, 7778 (2011).
14. N. C. Panoiu, X. F. Chen, and R. M. Osgood, Opt. Lett. **31**, 3609 (2006).
15. R. Claps, V. Raghunathan, D. Dimitropoulos, and B. Jalali, Opt. Express **11**, 2862 (2003).
16. M. R. E. Lamont, B. Luther-Davies, D. Y. Choi, S. Madden, X. Gai, and B. J. Eggleton, Opt. Express **16**, 20374 (2008).
17. B. Kuyken, X. P. Liu, R. M. Osgood Jr., R. Baets, G. Roelkens, and W. M. J. Green, Opt. Express **19**, 20172 (2011).
18. S. Pearl, N. Rotenberg, and H. M. van Driel, Appl. Phys. Lett. **93**, 131102 (2008).